Radial Basis Function Neural Network Models for Peak Stress and Strain in Plain Concrete under Triaxial Stress

Chao-Wei Tang[1]

Abstract: In the analysis or design process of reinforced concrete structures, the peak stress and strain in plain concrete under triaxial stress are critical. However, the nonlinear behavior of concrete under triaxial stresses is very complicated; modeling its behavior is therefore a complicated task. In the present study, several radial basis function neural network (RBFN) models have been developed for predicting peak stress and strain in plain concrete under triaxial stress. For the purpose of constructing the RBFN models, 56 records including normal- and high-strength concretes under triaxial loads were retrieved from literature for analysis. The *K*-means clustering algorithm and the pseudoinverse technique were employed to train the network for extracting knowledge from training examples. Besides, the performance of the developed RBFN models was estimated by the method of three-way data splits and *K*-fold cross-validation. On the other hand, a comparative study between the RBFN models and existing regression models was made. The results demonstrate the versatility of RBFN in constructing relationships among multiple variables of nonlinear behavior of concrete under triaxial stresses. Moreover, the results also show that the RBFN models provided better accuracy than the existing parametric models, both in terms of root-mean-square error and correlation coefficient.

DOI: 10.1061/(ASCE)MT.1943-5533.0000077

CE Database subject headings: Reinforced concrete; Stress; Strain; Neural networks; Concrete structures.

Author keywords: Concrete; Triaxial stress; Peak stress; Peak strain; Neural networks.

Introduction

The response of a reinforced concrete structure is determined substantially by the material response of the plain concrete of which it is composed. However, in many structural situations, concrete is subjected simultaneously to various stresses in a number of directions, such as a beam-column joint under axial load and biaxial bending. Hence in the analysis or design process of real three-dimensional reinforced concrete structures, a realistic representation of the multiaxial stress-strain curve or peak stress and strain of concrete is greatly required.

It is well known that concrete is a composite material, composed of aggregates of varying sizes embedded in a matrix of hardened cement paste; its strength is a function of the strength of aggregate, cement paste, admixtures used, and the interaction between the components. The stress-strain curves of the two principal components are essentially linear, except at very high stress levels (Mindness et al. 2003). Their differential response in concrete to an applied stress leads to inelastic behavior, and the stress-strain curve is highly nonlinear. In view of this, during the last few decades, there was a great effort aimed at developing analytical models that accurately predict the response of plain concrete to variable loading. Most early models focused on elasticity theory, yet more recently proposed models utilize general theories of solid mechanics including plasticity theory, damage theory, and fracture mechanics. By methods well described in the study of mechanics of materials, the multiaxial stress situation can be reduced to three normal stresses acting on three mutually perpendicular planes and thus ASTM C801 provides a standard test method for determining the mechanical properties of hardened concrete under triaxial loads.

The research on concrete under triaxial compressive loading is involving more and more investigators. A number of analytical models have been reported on the behavior of concrete under triaxial stress and the characteristic parameters for these models have been carefully examined since the 1980s (Ahamd and Shah 1982; Wang et al. 1987; Mander et al. 1988; Sheikh and Toklucu 1993; Cusson and Paultre 1995; El-Dash and Ahmad 1995; Menétrey and Willam 1996; Attard and Setunge 1996; Imran and Pantazopoulou 1996; Nielsen 1998; Razvi and Saatcioglu, 1999; Mei et al. 2001; Candappa et al. 2001; Sfer et al. 2002; Lokuge et al. 2005). Generally speaking, a multivariable nonlinear regression analysis is performed so that the major parameters (such as concrete strength, level of confining stress, moisture content, and load path) are calibrated to fit the experimental results and to derive the relationships among the involved parameters. However, the nonlinear behavior of concrete under triaxial stresses is very complicated; modeling its behavior is therefore a hard task. Besides, to apply the statistical approach in a complex nonlinear system is quite tough since choosing a fitting regression equation involves technique and experience. Hence it would be of interest to develop new methods that are easier, convenient, and

[1]Associate Professor, Dept. of Civil Engineering and Engineering Informatics, Cheng-Shiu Univ., No. 840, Chengcing Rd., Niaosong Township, Kaohsiung County, Taiwan. E-mail: tangcw@csu.edu.tw

Note. This manuscript was submitted on January 16, 2009; approved on December 14, 2009; published online on December 28, 2009. Discussion period open until February 1, 2011; separate discussions must be submitted for individual papers. This technical note is part of the ***Journal of Materials in Civil Engineering***, Vol. 22, No. 9, September 1, 2010. ©ASCE, ISSN 0899-1561/2010/9-923–934/$25.00.

more accurate than the existing methods in light of the availability of more experimental data and recent advance in the area of data analysis techniques.

As stated previously, traditional nonlinear regression analysis is obviously inadequate when it comes to modeling data that contains highly nonlinear characteristics. By contrast, an artificial neural network (ANN) is a powerful data-modeling tool that is able to capture and represent complex input-output relationships. Especially the true power and advantage of neural networks lies in their ability to represent nonlinear relationships and in their ability to learn these relationships directly from the data being modeled. Recent researches have shown that ANN-based modeling is an alternative method for modeling complex nonlinear relationship. As a result, ANN modeling techniques have been rapidly applied in such diverse fields as engineering, business, psychology, science, and medicine over the past few decades. During the last two decades, in civil engineering, the methodology of ANN has been successfully applied to model the structural behavior and properties of concrete materials such as strength, durability, expansion, and constitutive modeling (Ghaboussi et al. 1991; Yeh 1999; Zhao and Ren 2002; Tang et al. 2003, 2007; Jain et al. 2008).

ANN virtually consists of a number of processing elements (or artificial neurons) that are arranged logically into three or more layers and interact with each other via weighted connections to constitute a network. Therefore, ANN is a viable computational model for a wide variety of problems. The most commonly used ANN is probably the multilayer perceptrons (MLPs) network with back-propagation algorithm that uses the gradient-descent method to minimize the error between the network outputs and the target outputs (Rumelhart et al. 1986). However, for nonlinear modeling themes in real applications, MLP networks have poor process interpretability and are hindered by problems associated with weight optimization such as slow learning and local minimization (Jang et al. 1997). Since the 1990s, a special kind of neural network, i.e., the so-called radial basis function network (RBFN), has been applied as alternatives to alleviate some of the limitations of MLP networks (Bishop 1997).

In view of the above statements, this study aimed at investigating the application of RBFN in predicting the peak stress and its corresponding strain in plain concrete under triaxial stress. First, some fundamental aspects and mathematical equations for the nonlinear constitutive stress-strain relationships of confined concrete are introduced to highlight the difficulties associated with analytical model for hardened concrete under triaxial loads. Subsequently, a brief overview on the RBFN-based methodology for modeling is described. Then, 56 records including normal- and high-strength concretes were retrieved from existing literature (Attard and Setunge 1996; Imran and Pantazopoulou 1996) for analysis. Moreover, the calculated results were compared with the experimental values and with those determined from the Attard and Setunge (1996) and Richart et al. (1928) models.

Behavior of Concrete under Triaxial Stress

A lot of experiments have been executed to elaborate the theory of concrete facture under triaxial stresses. Most of these data are valid in particular for triaxial compressive stresses ($\sigma_1 > \sigma_2 = \sigma_3$), where σ_1, σ_2, and σ_3 are the maximum, intermediate, and minimum principal stresses, respectively, as shown schematically in Fig. 1. When conducting a triaxial test, hydrostatic pressure is often raised to some level and is then held constant until failure occurs under an increasing axial load. Presently, several prediction equations are available in the literature to predict the behavior of confined concrete. Among them, two prominent methods, which are selected and used in this study for comparison of the results from the neural networks, are outlined in the following.

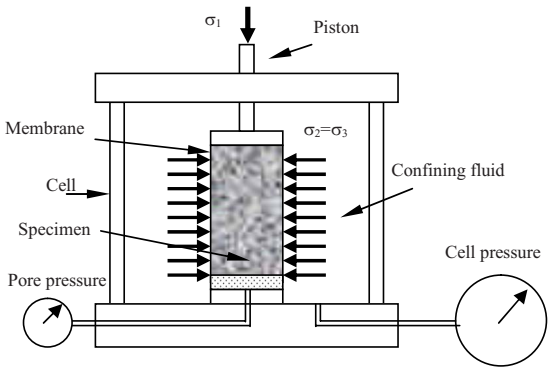

Fig. 1. Cylindrical triaxial test

Richart et al. Model

Richart et al. (1928) found that the strength and ductility of concrete are greatly increased under conditions of triaxial compression by uniform hydrostatic pressure. The incremental strength and ductility due to confinement can be expressed as follows:

$$f_{cc} = f_{cp} + 4.1 f_l \tag{1}$$

$$\varepsilon_{cc} = 5\varepsilon_{cp}\left(\frac{f_{cc}}{f_{cp}} - 0.8\right) \tag{2}$$

in which f_{cc}=maximum axial stress (or compressive strength) of confined concrete; f_{cp}=maximum axial stress of unconfined concrete; f_l=lateral confining pressure; ε_{cc}=axial compressive strain at peak stress of confined concrete; and ε_{cp}=axial compressive strain at peak stress of unconfined concrete.

Attard and Setunge Model

Attard and Setunge (1996) presented a strength criterion for the ultimate strength of confined concrete subjected to low confining pressure. The proposed formula extends into the tension-compression domain and is defined by

$$f_{cc} = f_{cp}\left(\frac{f_l}{f_t} + 1\right)^k \tag{3}$$

with

$$f_t = 0.288 f_{cp}^{0.67} \text{ MPa (for no silica fume concrete)}$$

$$= 0.558 f_{cp}^{0.5} \text{ MPa (for silica fume concrete)} \tag{4}$$

$$k = 1.25\left[1 + 0.062\frac{f_l}{f_{cp}}\right] f_{cp}^{-0.21} \tag{5}$$

where f_t=tensile strength of concrete and k=parameter that reflects the effectiveness of confinement. As for the strain at peak stress, the following equation is proposed:

Table 1. Experimental Data and Predicted Results of Various Models

							Experimental results		RBFN model		Richart et al. model		Attard and Setunge model			
Number	Mix	w/c	f_{cp} (MPa)	f_l (MPa)	ε_{cp}	E_c (MPa)	f_{cc} (MPa)	ε_{cc}	f_{RBF} (MPa)	ε_{RBF}	f_R (MPa)	ε_R	f_A (MPa)	ε_A	Type of subset	Source Ref.
1	aR	0.26	120.0	0.5	0.00300	55700	125	0.00260	126	0.00266	122	0.00363	124	0.00312	Training	Attard and
2				1.0	0.00300	55700	128	0.00290	129	0.00284	124	0.00400	129	0.00325	Training	Setunge
3				5.0	0.00300	55700	165	0.00380	158	0.00382	141	0.00863	158	0.00423	Training	(1996)
4				10.0	0.00300	55700	192	0.00530	192	0.00528	161	0.01200	187	0.00545	Training	
5				15.0	0.00300	55700	220	0.00600	217	0.00602	182	0.01550	212	0.00668	Training	
6				20.0	0.00300	55700	234	0.00800	231	0.00799	202	0.01725	235	0.00790	Training	
7	bR	0.30	120.0	5.0	0.00280	52800	168	0.00420	161	0.00420	141	0.00840	158	0.00394	Training	
8				10.0	0.00280	52800	187	0.00480	189	0.00480	161	0.01062	187	0.00509	Training	
9				15.0	0.00280	52800	211	0.00570	208	0.00570	182	0.01342	212	0.00623	Training	
10	cR	0.35	110.0	5.0	0.00280	55400	150	0.00350	148	0.00350	131	0.00789	147	0.00412	Training	
11				10.0	0.00280	55400	175	0.00440	174	0.00440	151	0.01107	175	0.00545	Training	
12				15.0	0.00280	55400	192	0.00600	192	0.00600	172	0.01324	200	0.00677	Training	
13	dR	0.26	100.0	1.0	0.00270	52900	106	0.00310	113	0.00315	104	0.00351	108	0.00300	Test	
14				5.0	0.00270	52900	121	0.00360	129	0.00295	121	0.00554	136	0.00419	Test	
15				10.0	0.00270	52900	144	0.00470	149	0.00405	141	0.00864	163	0.00567	Test	
16				15.0	0.00270	52900	165	0.00580	165	0.00589	162	0.01148	187	0.00716	Test	
17	aB	0.26	132.0	5.0	0.00340	49300	180	0.00500	170	0.00684	153	0.00958	171	0.00457	Validation	
18				10.0	0.00340	49300	200	0.00580	193	0.00732	173	0.01216	202	0.00574	Validation	
19				15.0	0.00340	49300	222	0.00780	213	0.00929	194	0.01499	228	0.00691	Validation	
20	dB	0.26	126.0	5.0	0.00340	49400	162	0.00500	165	0.00655	147	0.00826	164	0.00467	Validation	
21				10.0	0.00340	49400	186	0.00710	189	0.00702	167	0.01150	194	0.00595	Training	
22				15.0	0.00340	49400	211	0.00890	211	0.00900	188	0.01487	220	0.00722	Training	
23	aH	0.26	118.0	5.0	0.00280	57800	154	0.00380	159	0.00380	139	0.00707	156	0.00398	Training	
24				10.0	0.00280	57800	173	0.00490	185	0.00490	159	0.00933	185	0.00515	Training	
25				15.0	0.00280	57800	201	0.00620	203	0.00620	180	0.01265	210	0.00633	Training	
26	bH	0.30	110.0	5.0	0.00280	58700	153	0.00410	146	0.00410	131	0.00827	147	0.00412	Training	
27				10.0	0.00280	58700	164	0.00550	170	0.00550	151	0.00967	175	0.00545	Training	
28				15.0	0.00280	58700	185	0.00590	188	0.00590	172	0.01235	200	0.00677	Training	
29	cH	0.35	100.0	5.0	0.00260	54600	127	0.00390	130	0.00390	121	0.00611	136	0.00403	Training	
30				10.0	0.00260	54600	153	0.00520	146	0.00520	141	0.00949	163	0.00546	Training	
31				15.0	0.00260	54600	169	0.00750	159	0.00750	162	0.01157	187	0.00689	Training	
32	dH	0.26	96.0	5.0	0.00280	55800	119	0.00370	125	0.00370	117	0.00615	128	0.00444	Training	
33				10.0	0.00280	55800	147	0.00520	146	0.00520	137	0.01024	153	0.00608	Training	
34				15.0	0.00280	55800	157	0.00530	164	0.00530	158	0.01170	175	0.00772	Training	
35	eH	0.45	60.0	1.0	0.00210	45100	67	0.00270	89	0.00269	64	0.00333	67	0.00257	Training	
36				5.0	0.00210	45100	98	0.00480	100	0.00482	81	0.00875	89	0.00445	Training	
37				10.0	0.00210	45100	122	0.00760	114	0.00759	101	0.01295	112	0.00679	Training	
38				15.0	0.00210	45100	145	0.00990	130	0.00990	122	0.01698	132	0.00914	Training	
39	Batch 1	0.40	73.4	3.2	0.00325	37131	96	0.00495	96	0.00463	86	0.00830	94	0.00504	Training	Imran and
40				6.4	0.00325	37131	109	0.00650	106	0.00625	100	0.01108	111	0.00682	Training	Pantazopoulou
41				12.8	0.00325	37131	126	0.01045	128	0.01123	126	0.01483	139	0.01040	Training	(1996)
42				25.6	0.00325	37131	169	0.02050	171	0.02006	178	0.02435	186	0.01754	Training	
43				38.4	0.00325	37131	204	0.03105	206	0.03017	231	0.03218	225	0.02469	Training	
44				51.2	0.00325	37131	241	0.04090	230	0.04162	283	0.04028	261	0.03183	Training	
45	Batch 2	0.55	47.4	2.2	0.00280	34895	58	0.00430	58	0.00470	56	0.00583	61	0.00460	Training	
46				4.3	0.00280	34895	67	0.00690	65	0.00771	65	0.00868	72	0.00640	Training	
47				8.6	0.00280	34895	84	0.01460	81	0.01383	83	0.01349	92	0.00999	Training	
48				17.2	0.00280	34895	118	0.02530	117	0.02487	118	0.02367	125	0.01718	Training	
49				30.1	0.00280	34895	161	0.03600	170	0.03738	171	0.03637	167	0.02797	Training	
50				43.0	0.00280	34895	205	0.04730	215	0.04673	224	0.04926	206	0.03876	Training	
51	Batch 3	0.75	28.6	1.1	0.00260	26173	34	0.00470	36	0.00543	33	0.00486	35	0.00406	Training	
52				2.1	0.00260	26173	36	0.00675	39	0.00771	37	0.00612	41	0.00552	Training	
53				4.2	0.00260	26173	48	0.01385	46	0.01255	46	0.01144	51	0.00843	Training	
54				8.4	0.00260	26173	65	0.02375	62	0.02211	63	0.01919	69	0.01426	Training	
55				14.7	0.00260	26173	92	0.03425	87	0.03496	89	0.03151	93	0.02301	Training	
56				21.0	0.00260	26173	115	0.04460	114	0.04469	115	0.04161	116	0.03176	Training	

Range of parameters: w/c: 0.26–0.75; f_{cp}: 28.6–132.0 (MPa); f_{cc}: 33.6–240.5 (MPa); f_l: 0.5–51.2 (MPa); E_c: 26173–58700 (MPa); ε_{cp}: 0.00210–0.003400.00210–0.00340; ε_{cc}: 0.00260–0.04460

Note: w/c=water-cement (or binder) ratio; f_{cp}=maximum axial stress of unconfined concrete; f_l=lateral confining pressure; ε_{cp}=axial compressive strain at peak stress of unconfined concrete; E_c=modulus of elasticity of concrete; f_{cc}=maximum axial stress of confined concrete; ε_{cc}=axial compressive strain at peak stress of confined concrete; f_{RBF}=predicted peak stress using RK14-F4(4–11-1) model; ε_{RBF}=predicted peak strain using RK14-E4(4–11-1) model; f_R=predicted peak stress using Eq. (1); ε_R=predicted peak strain using Eq. (2); f_A=predicted peak stress using Eq. (3); ε_A=predicted peak strain using Eq. (6).

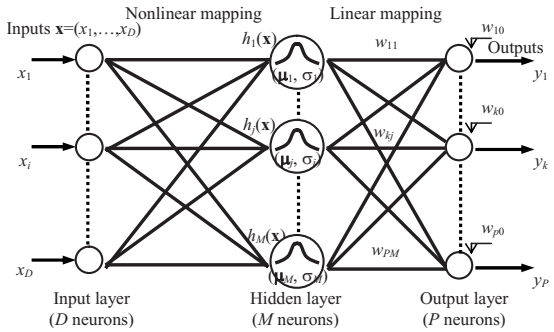

Fig. 2. Architecture of a typical RBFN

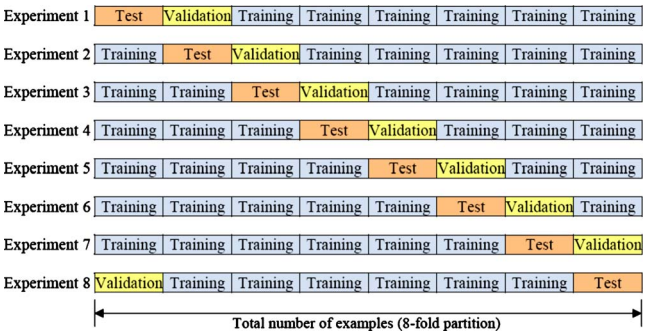

Fig. 3. Data set in eightfold partition

$$\varepsilon_{cc} = \varepsilon_{cp}\left[1 + (17 - 0.06f_{cp})\left(\frac{f_l}{f_{cp}}\right)\right] \tag{6}$$

RBFN Modeling of Concrete under Triaxial Stress

Fig. 2 shows the typical architecture of a RBFN with an input layer of D neurons, a hidden layer of M neurons, an output layer of P neurons, adjustable weights that exist only between the hidden and output layers, and biases at each output neuron. The input layer serves only as input distributor to the hidden layer, where they are transformed into a high-dimensional feature space using radial basis functions, called basis functions. The basis functions are exponentially decaying nonlinear functions and are radial functions, which have radial symmetry with respect to a center. The centers can be regarded as the neurons (or nodes) of the hidden layer. Each neuron in the hidden layer is a radial function. Then, the transformed data in this space are linearly transformed in order to approximate the target outputs. A commercially available software package, statistica Neural Networks, was used to establish RBFN models for predicting the peak stress and strain in plain concrete under triaxial stress. Details on the establishment of the RBFN models, along with sources of the data that are used in the development, are described below.

Data Set

The experimental data used in this study include 56 records, which are taken from the tests carried out by Attard and Setunge (1996) and Imran and Pantazopoulou (1996). The tests were done on cylindrical specimens using a triaxial cell and the stress path was followed in the conventional cylindrical triaxial test. In other words, axial compressive stress was gradually applied under displacement control, while the level of confining pressure was maintained. The complete list of the data is given in Table 1, where the name and the source of each specimen are referenced. To avoid the over-fit phenomenon, the so-called "three-way data splits" (i.e., divide the available data into training, validation, and test set) were adopted. Furthermore, in order to make the best use of limited data for training, model selection, and performance estimation, the method of K-fold cross validation was also adopted in the present study (Vapnik 1998). The data were randomly split into K equal parts and two different numbers of K were chosen (i.e., $K=8$ and $K=14$). For each of K experiments, K-2 folds were used for training, while the remaining twofolds were used for validation and testing, respectively. This procedure is illustrated in Fig. 3 for $K=8$.

Selection of Input and Output Variables for RBFN Models

Determining the network architecture is one of the most important tasks in the development of ANN models. Generally speaking, it requires the selection of the input and output parameters which will restrict the number of the input and output nodes of the network. Fortunately, selection of input variables for a network model could be guided by examining those parameters given in the aforementioned references since the existing empirical equations represent a survey of various statistical regression attempts for correlations between the behavior of confined concrete and characteristic parameters. Various RBFN models were considered for predicting peak stress, f_{cc}, and corresponding strain, ε_{cc}, in plain concrete under triaxial stress. After a series of simulations, it was found that the best input representation for the different output variables (i.e., f_{cc} and ε_{cc}) consisted of four variables: maximum axial stress of unconfined concrete, f_{cp}; lateral confining pressure, f_l; axial compressive strain at peak stress of unconfined concrete, ε_{cp}; and modulus of elasticity of concrete, E_c. The architectures of the developed ANN models for f_{cc} and ε_{cc} are shown separately in Table 2. The first column in Table 2 denotes the K-fold partition and the neural network structure for f_{cc}. For example, RK8-F1(4–10-1) stands for the RBFN model using the experiment 1 of eightfold partitions (see Fig. 3) and it has three layers (i.e., four input neurons in the first layer, one hidden layer with 10 hidden neurons in the second layer, and one output neuron in the third layer). In addition, several MLP models are also developed for comparison (see Table 2).

Network Topology and Training Algorithm

The training of a RBFN takes place in two distinct stages. Usually, the centers and width factors of the radial basis functions must be set, then the linear output layer is optimized. In the study, the centers stored in the radial hidden layer were optimized first using a kind of unsupervised training technique, i.e., the K-means method (Moody and Darken 1989). A set of data points was selected at random from the training data subset. These data points were the seeds of an incremental K-means clustering procedure and these K-means centers were used as centers in the RBFN. Then the width of the data was reflected in the radial deviations and deviations were assigned by the K-nearest neighbor method. In other words, each basis's deviation is individually set to the mean distance to its K nearest neighbors. Hence, deviations are smaller in tightly packed areas of space, preserving detail, and higher in sparse areas of space. After centers and deviations were set, the linear output layer was optimized using the pseudoinverse technique (Haykin 1999).

Table 2. Architecture of ANN Models

RBFN model for f_{cc}	Input variables	Output variable	RBFN model for ε_{cc}	Input variables	Output variable
RK8-F1(4–10-1)	$f_{cp}, f_l, \varepsilon_{cp}, E_c$	f_{cc}	RK8-E1(4–15-1)	$f_{cp}, f_l, \varepsilon_{cp}, E_c$	ε_{cc}
RK8-F2(4–18-1)	$f_{cp}, f_l, \varepsilon_{cp}, E_c$	f_{cc}	RK8-E2(4–16-1)	$f_{cp}, f_l, \varepsilon_{cp}, E_c$	ε_{cc}
RK8-F3(4–8-1)	$f_{cp}, f_l, \varepsilon_{cp}, E_c$	f_{cc}	RK8-E3(4–12-1)	$f_{cp}, f_l, \varepsilon_{cp}, E_c$	ε_{cc}
RK8-F4(4–5-1)	$f_{cp}, f_l, \varepsilon_{cp}, E_c$	f_{cc}	RK8-E4(4–11-1)	$f_{cp}, f_l, \varepsilon_{cp}, E_c$	ε_{cc}
RK8-F5(4–23-1)	$f_{cp}, f_l, \varepsilon_{cp}, E_c$	f_{cc}	RK8-E5(4–16-1)	$f_{cp}, f_l, \varepsilon_{cp}, E_c$	ε_{cc}
RK8-F6(4–4-1)	$f_{cp}, f_l, \varepsilon_{cp}, E_c$	f_{cc}	RK8-E6(4–9-1)	$f_{cp}, f_l, \varepsilon_{cp}, E_c$	ε_{cc}
RK8-F7(4–16-1)	$f_{cp}, f_l, \varepsilon_{cp}, E_c$	f_{cc}	RK8-E7(4–12-1)	$f_{cp}, f_l, \varepsilon_{cp}, E_c$	ε_{cc}
RK8-F8(4–7-1)	$f_{cp}, f_l, \varepsilon_{cp}, E_c$	f_{cc}	RK8-E8(4–11-1)	$f_{cp}, f_l, \varepsilon_{cp}, E_c$	ε_{cc}
RK14-F1(4–13-1)	$f_{cp}, f_l, \varepsilon_{cp}, E_c$	f_{cc}	RK14-E1(4–13-1)	$f_{cp}, f_l, \varepsilon_{cp}, E_c$	ε_{cc}
RK14-F2(4–14-1)	$f_{cp}, f_l, \varepsilon_{cp}, E_c$	f_{cc}	RK14-E2(4–15-1)	$f_{cp}, f_l, \varepsilon_{cp}, E_c$	ε_{cc}
RK14-F3(4–19-1)	$f_{cp}, f_l, \varepsilon_{cp}, E_c$	f_{cc}	RK14-E3(4–17-1)	$f_{cp}, f_l, \varepsilon_{cp}, E_c$	ε_{cc}
RK14-F4(4–11-1)	$f_{cp}, f_l, \varepsilon_{cp}, E_c$	f_{cc}	RK14-E4(4–11-1)	$f_{cp}, f_l, \varepsilon_{cp}, E_c$	ε_{cc}
RK14-F5(4–7-1)	$f_{cp}, f_l, \varepsilon_{cp}, E_c$	f_{cc}	RK14-E5(4–6-1)	$f_{cp}, f_l, \varepsilon_{cp}, E_c$	ε_{cc}
RK14-F6(4–8-1)	$f_{cp}, f_l, \varepsilon_{cp}, E_c$	f_{cc}	RK14-E6(4–5-1)	$f_{cp}, f_l, \varepsilon_{cp}, E_c$	ε_{cc}
RK14-F7(4–11-1)	$f_{cp}, f_l, \varepsilon_{cp}, E_c$	f_{cc}	RK14-E7(4–11-1)	$f_{cp}, f_l, \varepsilon_{cp}, E_c$	ε_{cc}
RK14-F8(4–6-1)	$f_{cp}, f_l, \varepsilon_{cp}, E_c$	f_{cc}	RK14-E8(4–12-1)	$f_{cp}, f_l, \varepsilon_{cp}, E_c$	ε_{cc}
RK14-F9(4–14-1)	$f_{cp}, f_l, \varepsilon_{cp}, E_c$	f_{cc}	RK14-E9(4–11-1)	$f_{cp}, f_l, \varepsilon_{cp}, E_c$	ε_{cc}
RK14-F10(4–21-1)	$f_{cp}, f_l, \varepsilon_{cp}, E_c$	f_{cc}	RK14-E10(4–12-1)	$f_{cp}, f_l, \varepsilon_{cp}, E_c$	ε_{cc}
RK14-F11(4–15-1)	$f_{cp}, f_l, \varepsilon_{cp}, E_c$	f_{cc}	RK14-E11(4–6-1)	$f_{cp}, f_l, \varepsilon_{cp}, E_c$	ε_{cc}
RK14-F12(4–10-1)	$f_{cp}, f_l, \varepsilon_{cp}, E_c$	f_{cc}	RK14-E12(4–12-1)	$f_{cp}, f_l, \varepsilon_{cp}, E_c$	ε_{cc}
RK14-F13(4–10-1)	$f_{cp}, f_l, \varepsilon_{cp}, E_c$	f_{cc}	RK14-E13(4–10-1)	$f_{cp}, f_l, \varepsilon_{cp}, E_c$	ε_{cc}
RK14-F14(4–18-1)	$f_{cp}, f_l, \varepsilon_{cp}, E_c$	f_{cc}	RK14-E14(4–14-1)	$f_{cp}, f_l, \varepsilon_{cp}, E_c$	ε_{cc}
RK14-F4(3–7-1)	$f_{cp}, f_l, \varepsilon_{cpc}$	f_{cc}	RK14-E4(3–7-1)	$f_{cp}, f_l, \varepsilon_{cpc}$	ε_{cc}
RK14-F4(2–7-1)	f_{cp}, f_l	f_{cc}	RK14-E4(2–12-1)	f_{cp}, f_l	ε_{cc}

MLP model for f_{cc}	Input variables	Output variable	MLP model for ε_{cc}	Input variables	Output variable
MK8-F1(4–10-1)	$f_{cp}, f_l, \varepsilon_{cp}, E_c$	f_{cc}	MK8-E1(4–8-1)	$f_{cp}, f_l, \varepsilon_{cp}, E_c$	ε_{cc}
MK8-F2(4–4-1)	$f_{cp}, f_l, \varepsilon_{cp}, E_c$	f_{cc}	MK8-E2(4–5-1)	$f_{cp}, f_l, \varepsilon_{cp}, E_c$	ε_{cc}
MK8-F3(4–4-1)	$f_{cp}, f_l, \varepsilon_{cp}, E_c$	f_{cc}	MK8-E3(4–7-1)	$f_{cp}, f_l, \varepsilon_{cp}, E_c$	ε_{cc}
MK8-F4(4–6-1)	$f_{cp}, f_l, \varepsilon_{cp}, E_c$	f_{cc}	MK8-E4(4–5-1)	$f_{cp}, f_l, \varepsilon_{cp}, E_c$	ε_{cc}
MK8-F5(4–9-1)	$f_{cp}, f_l, \varepsilon_{cp}, E_c$	f_{cc}	MK8-E5(4–2-1)	$f_{cp}, f_l, \varepsilon_{cp}, E_c$	ε_{cc}
MK8-F6(4–5-1)	$f_{cp}, f_l, \varepsilon_{cp}, E_c$	f_{cc}	MK8-E6(4–5-1)	$f_{cp}, f_l, \varepsilon_{cp}, E_c$	ε_{cc}
MK8-F7(4–11-1)	$f_{cp}, f_l, \varepsilon_{cp}, E_c$	f_{cc}	MK8-E7(4–7-1)	$f_{cp}, f_l, \varepsilon_{cp}, E_c$	ε_{cc}
MK8-F8(4–11-1)	$f_{cp}, f_l, \varepsilon_{cp}, E_c$	f_{cc}	MK8-E8(4–8-1)	$f_{cp}, f_l, \varepsilon_{cp}, E_c$	ε_{cc}
MK14-F1(4–17-1)	$f_{cp}, f_l, \varepsilon_{cp}, E_c$	f_{cc}	MK14-E1(4–5-1)	$f_{cp}, f_l, \varepsilon_{cp}, E_c$	ε_{cc}
MK14-F2(4–6-1)	$f_{cp}, f_l, \varepsilon_{cp}, E_c$	f_{cc}	MK14-E2(4–5-1)	$f_{cp}, f_l, \varepsilon_{cp}, E_c$	ε_{cc}
MK14-F3(4–11-1)	$f_{cp}, f_l, \varepsilon_{cp}, E_c$	f_{cc}	MK14-E3(4–6-1)	$f_{cp}, f_l, \varepsilon_{cp}, E_c$	ε_{cc}
MK14-F4(4–12-1)	$f_{cp}, f_l, \varepsilon_{cp}, E_c$	f_{cc}	MK14-E4(4–6-1)	$f_{cp}, f_l, \varepsilon_{cp}, E_c$	ε_{cc}
MK14-F5(4–8-1)	$f_{cp}, f_l, \varepsilon_{cp}, E_c$	f_{cc}	MK14-E5(4–5-1)	$f_{cp}, f_l, \varepsilon_{cp}, E_c$	ε_{cc}
MK14-F6(4–5-1)	$f_{cp}, f_l, \varepsilon_{cp}, E_c$	f_{cc}	MK14-E6(4–6-1)	$f_{cp}, f_l, \varepsilon_{cp}, E_c$	ε_{cc}
MK14-F7(4–8-1)	$f_{cp}, f_l, \varepsilon_{cp}, E_c$	f_{cc}	MK14-E7(4–7-1)	$f_{cp}, f_l, \varepsilon_{cp}, E_c$	ε_{cc}
MK14-F8(4–6-1)	$f_{cp}, f_l, \varepsilon_{cp}, E_c$	f_{cc}	MK14-E8(4–7-1)	$f_{cp}, f_l, \varepsilon_{cp}, E_c$	ε_{cc}
MK14-F9(4–6-1)	$f_{cp}, f_l, \varepsilon_{cp}, E_c$	f_{cc}	MK14-E9(4–5-1)	$f_{cp}, f_l, \varepsilon_{cp}, E_c$	ε_{cc}
MK14-F10(4–4-1)	$f_{cp}, f_l, \varepsilon_{cp}, E_c$	f_{cc}	MK14-E10(4–3-1)	$f_{cp}, f_l, \varepsilon_{cp}, E_c$	ε_{cc}
MK14-F11(4–7-1)	$f_{cp}, f_l, \varepsilon_{cp}, E_c$	f_{cc}	MK14-E11(4–2-1)	$f_{cp}, f_l, \varepsilon_{cp}, E_c$	ε_{cc}
MK14-F12(4–8-1)	$f_{cp}, f_l, \varepsilon_{cp}, E_c$	f_{cc}	MK14-E12(4–6-1)	$f_{cp}, f_l, \varepsilon_{cp}, E_c$	ε_{cc}
MK14-F13(4–6-1)	$f_{cp}, f_l, \varepsilon_{cp}, E_c$	f_{cc}	MK14-E13(4–14-1)	$f_{cp}, f_l, \varepsilon_{cp}, E_c$	ε_{cc}
MK14-F14(4–13-1)	$f_{cp}, f_l, \varepsilon_{cp}, E_c$	f_{cc}	MK14-E14(4–4-1)	$f_{cp}, f_l, \varepsilon_{cp}, E_c$	ε_{cc}
MK14-F4(3–7-1)	$f_{cp}, f_l, \varepsilon_{cp}$	f_{cc}	MK14-E4(3–6-1)	$f_{cp}, f_l, \varepsilon_{cp}$	ε_{cc}
MK14-F4(2–5-1)	f_{cp}, f_l	f_{cc}	MK14-E4(2–2-1)	f_{cp}, f_l	ε_{cc}

As previously mentioned, the data set was divided into three subsets: training, validation, and test cases. To reiterate, the neural networks were trained using the training subset only. The validation subset was used to keep an independent check on the performance of the networks during training, with deterioration in the validation errors indicating overlearning. If overlearning occurs, the software stops training the network and restores it to the state with minimum validation error. The validation error was also used by the software to select between the available networks. However, if a large number of networks are tested, a random sampling

Table 3. Summary of RMS Error and Pearson Correlation Coefficient for f_{cc}

	RMS error (MPa)			Pearson correlation coefficient		
ANN model	Training subset	Validation subset	Test subset	Training subset	Validation subset	Test subset
RK8-F1(4–10-1)	8.93	6.62	18.86	0.9853	0.9903	0.9865
RK8-F2(4–18-1)	6.55	5.85	3.38	0.9924	0.9850	0.9956
RK8-F3(4–8-1)	10.90	10.21	6.38	0.9800	0.9680	0.9741
RK8-F4(4–5-1)	16.19	16.39	9.45	0.9556	0.9463	0.9815
RK8-F5(4–23-1)	2.50	10.43	13.74	0.9990	0.9070	0.9203
RK8-F6(4–4-1)	7.28	9.48	17.60	0.9614	0.9895	0.9485
RK8-F7(4–16-1)	6.51	26.84	31.07	0.9847	0.9962	0.9248
RK8-F8(4–7-1)	7.23	13.14	21.25	0.9859	0.9643	0.9836
Average	8.26	12.37	15.22	0.9805	0.9683	0.9644
RK14-F1(4–13-1)	6.16	4.79	9.70	0.9927	0.9864	0.9907
RK14-F2(4–14-1)	3.52	5.95	10.28	0.9975	0.9997	0.9852
RK14-F3(4–19-1)	6.92	5.89	2.81	0.9915	0.9998	0.9987
RK14-F4(4–11-1)	6.19	7.63	5.92	0.9930	0.9807	0.9967
RK14-F5(4–7-1)	12.76	6.47	6.48	0.9686	0.9896	0.9707
RK14-F6(4–8-1)	8.74	6.75	4.71	0.9861	0.9783	0.9951
RK14-F7(4–11-1)	7.34	5.53	8.44	0.9906	0.9887	0.9770
RK14-F8(4–6-1)	11.18	17.00	9.22	0.9774	0.9721	0.9399
RK14-F9(4–14-1)	1.39	14.47	8.26	0.9997	0.9665	0.9949
RK14-F10(4–21-1)	4.48	10.10	17.75	0.9962	0.9893	0.9861
RK14-F11(4–15-1)	5.54	4.20	13.29	0.9934	0.9989	0.9831
RK14-F12(4–10-1)	8.25	10.96	2.92	0.9825	0.9986	0.9995
RK14-F13(4–10-1)	8.23	10.38	17.22	0.9823	0.9988	1.0000
RK14-F14(4–18-1)	5.99	14.86	13.77	0.9928	0.9825	0.9969
RK14-F1(4–13-1)	6.91	8.93	9.34	0.9872	0.9869	0.9818
Average	6.16	4.79	9.70	0.9927	0.9864	0.9907
MK8-F1(4–10-1)	5.38	6.93	13.49	0.9943	0.9819	0.9910
MK8-F2(4–4-1)	9.37	5.00	8.76	0.9863	0.9957	0.9795
MK8-F3(4–4-1)	9.39	4.02	8.15	0.9843	0.9816	0.9675
MK8-F4(4–6-1)	13.42	3.58	10.59	0.9833	0.9938	0.9650
MK8-F5(4–9-1)	8.67	4.35	10.95	0.9877	0.9886	0.9924
MK8-F6(4–5-1)	10.12	3.28	5.44	0.9824	0.9988	0.9808
MK8-F7(4–11-1)	9.77	1.23	8.36	0.9698	0.9998	0.9994
MK8-F8(4–11-1)	5.91	9.97	9.06	0.9908	0.9867	0.9984
Average	9.00	4.80	9.35	0.9849	0.9909	0.9843
MK14-F1(4–17-1)	15.07	5.07	17.80	0.9932	0.9884	0.9930
MK14-F2(4–6-1)	8.32	2.57	12.04	0.9860	0.9981	0.9699
MK14-F3(4–11-1)	10.99	3.08	14.81	0.9873	0.9991	0.9978
MK14-F4(4–12-1)	8.08	2.19	12.22	0.9889	0.9983	0.9991
MK14-F5(4–8-1)	7.53	2.31	3.95	0.9892	0.9941	0.9925
MK14-F6(4–5-1)	9.31	3.37	6.14	0.9842	0.9844	0.9909
MK14-F7(4–8-1)	8.68	3.27	8.01	0.9868	0.9913	0.9918
MK14-F8(4–6-1)	7.61	5.99	5.80	0.9898	0.9869	0.9939
MK14-F9(4–6-1)	7.16	9.18	8.09	0.9915	0.9826	0.9866
MK14-F10(4–4-1)	12.23	2.00	7.06	0.9752	0.9989	0.9965
MK14-F11(4–7-1)	10.29	0.37	18.20	0.9789	0.9999	0.9995
MK14-F12(4–8-1)	8.83	0.91	5.94	0.9799	0.9999	1.0000
MK14-F13(4–6-1)	7.50	0.53	3.76	0.9853	0.9998	0.9989
MK14-F14(4–13-1)	6.68	8.02	2.51	0.9912	0.9934	0.9998
Average	9.16	3.49	9.02	0.9882	0.9926	0.9911
RK14-F4(3–7-1)	11.10	5.58	12.57	0.9774	0.9854	0.9996
RK14-F4(2–7-1)	9.70	3.73	9.03	0.9828	0.9929	0.9990
MK14-F4(3–7-1)	6.28	3.22	10.30	0.9929	0.9906	0.9991
MK14-F4(2–5-1)	7.78	3.36	9.57	0.9889	0.9901	0.9983

Table 4. Summary of RMS Error and Pearson Correlation Coefficient for ε_{cc}

	RMS error			Pearson correlation coefficient		
ANN model	Training subset	Validation subset	Test subset	Training subset	Validation subset	Test subset
RK8-E1(4–15-1)	0.00238	0.00067	0.00128	0.9505	0.9841	0.9897
RK8-E2(4–16-1)	0.00315	0.00071	0.00052	0.9664	0.9083	0.9354
RK8-E3(4–12-1)	0.00265	0.00109	0.00107	0.9770	0.9738	0.8635
RK8-E4(4–11-1)	0.00398	0.00069	0.00107	0.9555	0.9211	0.9666
RK8-E5(4–16-1)	0.00078	0.00314	0.00156	0.9980	0.9058	0.9106
RK8-E6(4–9-1)	0.00226	0.00427	0.00528	0.9742	0.9793	0.9872
RK8-E7(4–12-1)	0.00045	0.01631	0.00972	0.9879	0.9448	0.9563
RK8-E8(4–11-1)	0.00144	0.00059	0.00941	0.9861	0.9717	0.9147
Average	0.00214	0.00343	0.00374	0.9744	0.9486	0.9405
RK14-E1(4–13-1)	0.00260	0.00060	0.00121	0.9750	0.9839	0.9745
RK14-E2(4–15-1)	0.00224	0.00036	0.00132	0.9816	0.9844	0.9647
RK14-E3(4–17-1)	0.00281	0.00077	0.00077	0.9706	0.9929	0.9321
RK14-E4(4–11-1)	0.00050	0.00160	0.00046	0.9991	0.9943	0.9523
RK14-E5(4–6-1)	0.00341	0.00099	0.00109	0.9494	0.9888	0.9641
RK14-E6(4–5-1)	0.00412	0.00270	0.00241	0.9371	0.9651	0.9988
RK14-E7(4–11-1)	0.00218	0.00118	0.00305	0.9827	0.9651	0.8319
RK14-E8(4–12-1)	0.00220	0.00124	0.00067	0.9821	0.9059	0.9208
RK14-E9(4–11-1)	0.00262	0.00176	0.00128	0.9750	0.9956	0.9043
RK14-E10(4–12-1)	0.00276	0.00288	0.00478	0.9649	0.9861	0.9746
RK14-E11(4–6-1)	0.00205	0.00161	0.00408	0.9796	0.9965	0.9548
RK14-E12(4–12-1)	0.00119	0.00554	0.00157	0.9922	0.9981	0.9942
RK14-E13(4–10-1)	0.00156	0.00656	0.00104	0.9766	0.9948	0.9958
RK14-E14(4–14-1)	0.00090	0.00009	0.01312	0.9958	0.9974	0.9945
RK14-E1(4–13-1)	0.00222	0.00199	0.00263	0.9722	0.9726	0.9424
Average	0.00260	0.00060	0.00121	0.9750	0.9839	0.9745
MK8-E1(4–8-1)	0.00146	0.00025	0.00066	0.9932	0.9703	0.9905
MK8-E2(4–5-1)	0.00307	0.00042	0.00061	0.9685	0.9387	0.9569
MK8-E3(4–7-1)	0.00148	0.00033	0.00094	0.9929	0.9869	0.9568
MK8-E4(4–5-1)	0.00189	0.00052	0.00080	0.9882	0.9311	0.9716
MK8-E5(4–2-1)	0.00205	0.00116	0.00168	0.9868	0.9768	0.8900
MK8-E6(4–5-1)	0.00098	0.00112	0.00221	0.9952	0.9965	0.9828
MK8-E7(4–7-1)	0.00064	0.00435	0.00216	0.9767	0.9954	0.9940
MK8-E8(4–8-1)	0.00106	0.00026	0.00866	0.9926	0.9919	0.9878
Average	0.00158	0.00105	0.00222	0.9868	0.9734	0.9663
MK14-E1(4–5-1)	0.00116	0.00037	0.00050	0.9951	0.9674	0.9974
MK14-E2(4–5-1)	0.00138	0.00022	0.00077	0.9932	0.9819	0.9475
MK14-E3(4–6-1)	0.00295	0.00014	0.00045	0.9677	0.9971	0.9926
MK14-E4(4–6-1)	0.00143	0.00026	0.00090	0.9927	0.9730	0.9917
MK14-E5(4–5-1)	0.00183	0.00021	0.00087	0.9880	0.9942	0.9692
MK14-E6(4–6-1)	0.00140	0.00021	0.00117	0.9931	0.9670	0.9873
MK14-E7(4–7-1)	0.00155	0.00024	0.00041	0.9912	0.9891	0.9676
MK14-E8(4–7-1)	0.00129	0.00045	0.00114	0.9929	0.9745	0.9163
MK14-E9(4–5-1)	0.00190	0.00040	0.00133	0.9869	0.9850	0.9233
MK14-E10(4–3-1)	0.00142	0.00068	0.00260	0.9931	0.9993	0.9938
MK14-E11(4–2-1)	0.00048	0.00110	0.00190	0.9963	0.9987	0.9992
MK14-E12(4–6-1)	0.00089	0.00299	0.00363	0.9975	0.9946	0.9971
MK14-E13(4–14-1)	0.00095	0.00128	0.00468	0.9913	0.9966	0.9957
MK14-E14(4–4-1)	0.00198	0.00007	0.00980	0.9799	0.9977	0.9918
Average	0.00147	0.00062	0.00215	0.9892	0.9805	0.9712
RK14-E4(3–7-1)	0.00338	0.00165	0.00126	0.9576	0.9633	0.9928
RK14-E4(2–12-1)	0.00141	0.00028	0.00061	0.9927	0.9974	0.9889
MK14-E4(3–6-1)	0.00156	0.00023	0.00140	0.9911	0.9797	0.9939
MK14-E4(2–2-1)	0.00208	0.00035	0.00153	0.9843	0.9518	0.9882

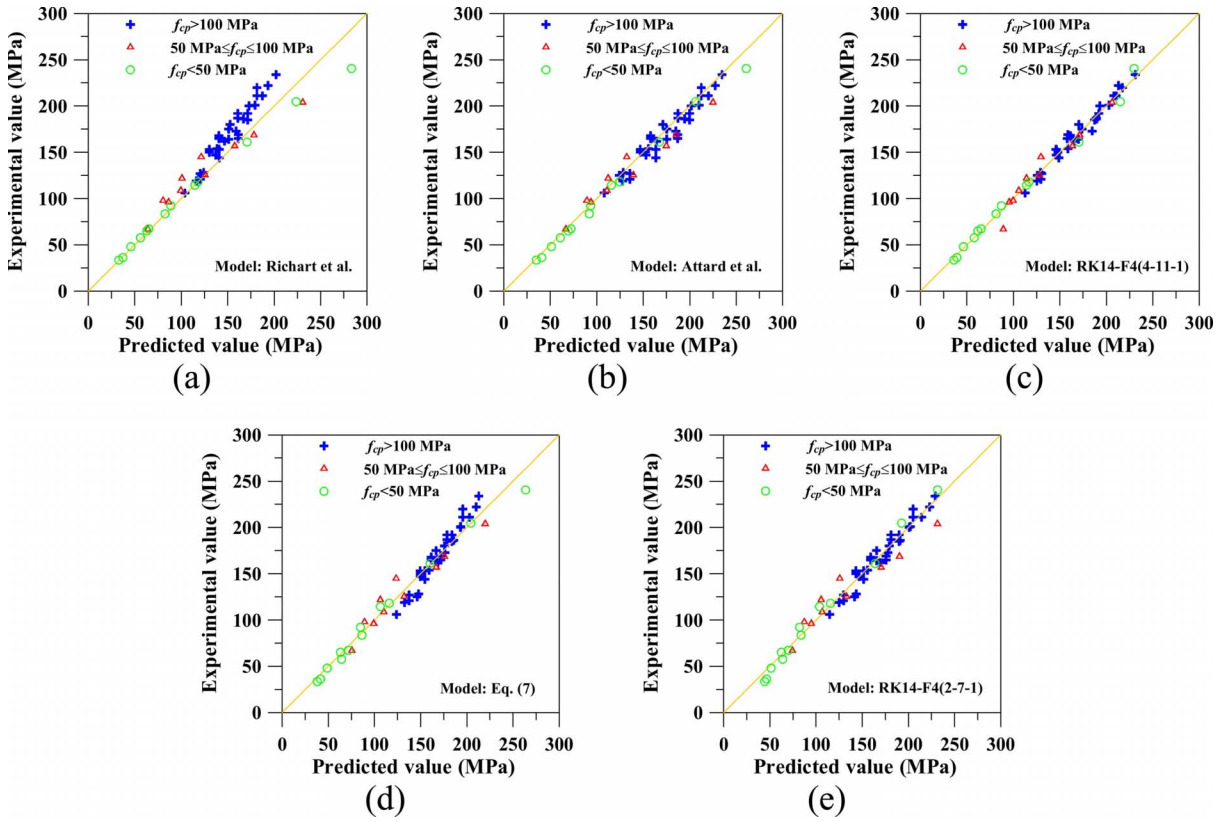

Fig. 4. Experimental versus predicted peak stresses of confined concrete

effect can kick in and one may get a network with a good validation error which is not actually indicative of good generalization capabilities. Therefore, a third subset (i.e., the test subset) was maintained and one could visually inspect performance after training.

A great amount of networks were tested. The best network found for a great diversity of ANN models was retained. The performance of the developed ANN was measured in two aspects: one is the value of root-mean-square (RMS) error of the network output to the target output and the other is the Pearson correlation coefficient, r, between the network output and the target output. In principle, the lower the RMS error value or the higher the r value is, the better the prediction relationship will be. Judging from Tables 3 and 4, it can be concluded that the developed RBFN models had a good generalization performance in terms of the average RMS error and r values obtained from the K-fold cross-validation with $K=14$. Especially, the average r values for the training, validation, and testing subsets are all greater than 0.97 (see Tables 3 and 4). The results demonstrate the peak stress and strain in plain concrete under triaxial stress can be accurately estimated using four input variables (i.e., f_{cp}, f_l, ε_{cp}, and E_c). This is quite consistent with most existing analytical methods. Besides, as compared with MLPs (refer to Tables 3 and 4), RBFNs not only trained quite rapidly during training but also provided fairly good accuracy.

Comparison with Empirical Equations

In order to evaluate the capabilities of RBFNs in predicting the peak stress and strain of plain concrete under triaxial stress, two developed RBFN models [i.e., RK14-F4(4–11-1) for f_{cc} and RK14-E4(4–11-1) for ε_{cc}] were chosen. A comparison of the predicated results obtained with the two RBFN models and the aforementioned empirical equations are given in Table 1. In Table 1, all models used the same training, validation, and testing data to calculate the predicted peak stress, f_{ccp}, and its corresponding axial strain, ε_{ccp}, in confined concrete. Regarding all 56 specimens, the experimental peak stress (f_{cce} collected from the literature) is plotted against the predicted values, as shown in Figs. 4(a–c). To show the overall trend of correlation, the theoretical line with $f_{cce}/f_{ccp}=1$ was drawn on the graphs along with the data points plotted. The nearer the points gather around the diagonal line, the better are the predicted values. Figs. 4(a and b) show that the correlation between the values of f_{cce} and f_{ccp} was deemed satisfactory for the weaker specimens by Eqs. (1) and (3), while the correlation for the stronger specimens was more scattered, particularly by Eq. (1). By contrast, Fig. 4(c) clearly shows that the less scatter of data around the diagonal line confirms the fact that neural network-based model is an excellent predictor for the value of f_{cc}. Overall, it can be observed that a larger variation in the accuracy was noticed in the Richart et al. model. Therefore, based on the 56 records, an improved equation for Eq. (1) is proposed as follows:

$$f_{cc} = 1.2f_{cp} + 3.4f_l \tag{7}$$

where the parameters are as previously defined. The coefficient of determination, R^2, of Eq. (7) is 0.97 and thus a superior f_{cce} versus f_{ccp} plot is obtained, as shown in Fig. 4(d).

As for the axial compressive strain at peak stress of confined concrete, the experimental strain (ε_{cce} collected from the literature) is also plotted against the predicted values (ε_{ccp}), as shown in Fig. 5. It is evident from Figs. 5(a and b) that the correlation between the values of ε_{cce} and ε_{ccp} was less than satisfactory

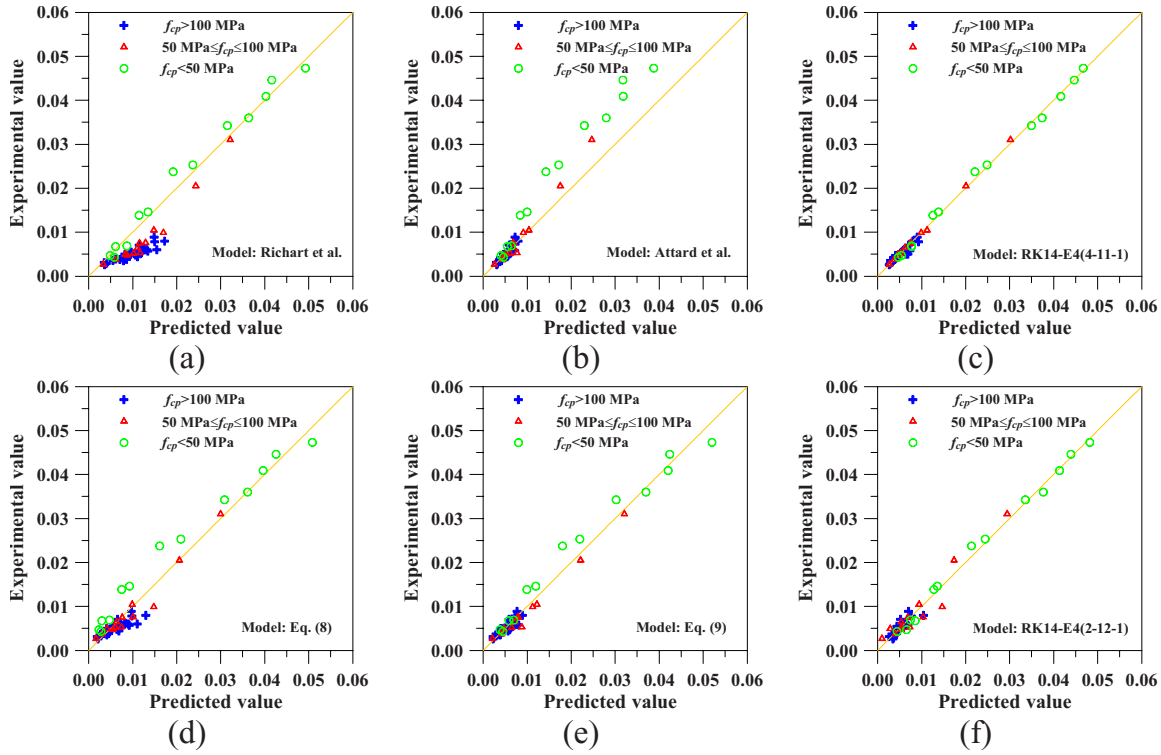

Fig. 5. Experimental versus predicted axial compressive strains at peak stress of confined concrete

by Eqs. (2) and (6). As expected, the neural network approach provides better results [Fig. 5(c)]. Similarly, based on the 56 records, the following modified equations are proposed separately for Eqs. (2) and (6):

$$\varepsilon_{cc} = 0.68\varepsilon_{cp} + 8.1\varepsilon_{cp}\left[\ln\left(\frac{f_{cc}}{f_{cp}}\right)\right]^2 \tag{8}$$

$$\varepsilon_{cc} = 1.39\varepsilon_{cp}\left[0.50 + (17 - 0.06f_{cp})\left(\frac{f_l}{f_{cp}}\right)\right] \tag{9}$$

where the parameters are as previously defined. The R^2 values for Eqs. (8) and (9) are 0.94 and 0.98, respectively. Consequently, better ε_{cce} versus ε_{ccp} plots are obtained [Figs. 5(d and e)].

Furthermore, for comparison purpose, the values of RMS error and r for the entire data set in various models are listed in Table 5. For example, the values of RMS error and r by RK14-F4(4–11-1) model were 6.28 MPa and 0.9924, while by RK14-E4(4–11-1) model were 0.00065 and 0.9983. Concurrently considering the peak stress and the corresponding strain, the overall predictions from the RBFN models were found to be better than the aforementioned parametric models and the proposed regression models. This indicates that the use of RBFN is an appropriate and powerful tool for predicting the peak stress and strain in normal- and high-strength concrete under triaxial stress.

Computational Simulation of Peak Stress and Strain in Concrete

Having trained a reliable neural network, one can use it to make predictions on new data. However, the trained model is implicit and hidden in the network structure as well as the optimized weights between the nodes. Therefore, computational simulation of peak stress and strain in concrete under triaxial stress was performed using the trained RBFN models.

The relative importance of the input variables used can be examined by the so-called sensitivity analysis. In sensitivity

Table 5. Comparison between Various Models

Model for f_{cc}			Model for ε_{cc}		
Model	RMS (MPa)	r	Model	RMS	r
Model: Eq. (1)	17.91	0.9561	Model: Eq. (2)	0.00460	0.9626
Model: Eq. (3)	9.58	0.9875	Model: Eq. (6)	0.00376	0.9878
Model: Eq. (7)	10.46	0.9789	Model: Eq. (8)	0.00170	0.9883
RK14-F4(4–11-1)	6.28	0.9924	RK14-E4(4–11-1)	0.00065	0.9983
RK14-F4(3–7-1)	10.91	0.9769	RK14-E4(3–7-1)	0.00318	0.9581
RK14-F4(2–7-1)	9.36	0.9831	RK14-E4(2–12-1)	0.00132	0.9929

Note: RMS=root-mean-square error; r=Pearson correlation coefficient.

Table 6. Sensitivity Analysis of Input Variables

	Rank of variable									Rank of variable							
	Training subset				Training subset					Training subset				Training subset			
ANN model for f_{cc}	f_{cp}	f_l	ε_{cp}	E_c	f_{cp}	f_l	ε_{cp}	E_c	ANN model for ε_{cc}	f_{cp}	f_l	ε_{cp}	E_c	f_{cp}	f_l	ε_{cp}	E_c
RK8-F1(4–10-1)	1	2	3	4	1	2	3	4	RK8-E1(4–15-1)	2	1	4	3	3	2	4	1
RK8-F2(4–18-1)	2	1	4	3	1	2	3	4	RK8-E2(4–16-1)	3	1	4	2	2	1	4	3
RK8-F3(4–8-1)	2	1	4	3	1	2	3	4	RK8-E3(4–12-1)	3	1	4	2	4	2	3	1
RK8-F4(4–5-1)	2	1	4	3	3	1	2	4	RK8-E4(4–11-1)	3	1	4	2	4	3	1	2
RK8-F5(4–23-1)	2	1	4	3	3	1	2	4	RK8-E5(4–16-1)	3	1	4	2	3	1	4	2
RK8-F6(4–4-1)	2	1	4	3	2	1	4	3	RK8-E6(4–9-1)	3	1	4	2	4	1	3	2
RK8-F7(4–16-1)	1	2	3	4	1	2	4	3	RK8-E7(4–12-1)	3	1	4	2	3	1	4	2
RK8-F8(4–7-1)	1	2	3	4	1	2	4	3	RK8-E8(4–11-1)	3	1	4	2	4	1	3	2
RK14-F1(4–13-1)	2	1	4	3	1	2	3	4	RK14-E1(4–13-1)	2	1	4	3	3	2	4	1
RK14-F2(4–14-1)	1	2	4	3	1	2	4	3	RK14-E2(4–15-1)	2	1	4	3	1	3	4	2
RK14-F3(4–19-1)	1	2	4	3	2	1	4	3	RK14-E3(4–17-1)	2	1	4	3	3	4	2	1
RK14-F4(4–11-1)	2	1	4	3	1	2	3	4	RK14-E4(4–11-1)	3	1	4	2	1	4	2	3
RK14-F5(4–7-1)	1	2	4	3	1	2	4	3	RK14-E5(4–6-1)	4	1	3	2	1	3	4	2
RK14-F6(4–8-1)	1	2	4	3	1	2	4	3	RK14-E6(4–5-1)	2	1	4	3	3	2	4	1
RK14-F7(4–11-1)	2	1	4	3	1	2	4	3	RK14-E7(4–11-1)	3	1	4	2	4	2	3	1
RK14-F8(4–6-1)	2	1	4	3	3	1	2	4	RK14-E8(4–12-1)	3	1	4	2	4	1	3	2
RK14-F9(4–14-1)	1	2	4	3	2	1	4	3	RK14-E9(4–11-1)	3	1	4	2	1	2	3	4
RK14-F10(4–21-1)	1	2	4	3	3	1	2	4	RK14-E10(4–12-1)	2	1	4	3	2	1	4	3
RK14-F11(4–15-1)	2	1	4	3	1	3	4	2	RK14-E11(4–6-1)	3	1	4	2	3	1	4	2
RK14-F12(4–10-1)	2	1	3	4	2	1	4	3	RK14-E12(4–12-1)	3	1	4	2	3	1	4	2
RK14-F13(4–10-1)	2	1	4	3	1	3	4	2	RK14-E13(4–10-1)	2	1	4	3	3	2	4	1
RK14-F14(4–18-1)	2	1	4	3	2	1	3	4	RK14-E14(4–14-1)	2	1	4	3	2	3	4	1

Note: The smaller the number of rank, the more important the variable.

analysis, the data set is submitted to the network repeatedly, with each variable in turn treated as missing, and the resulting network error is recorded. If an important variable is removed in this fashion, the error will increase a great deal; if an unimportant variable is removed, the error will not increase very much. The sensitivity analysis of the RBFN models shows that lateral confining pressure, f_l, and maximum axial stress of unconfined concrete, f_{cp}, were the main influential factors in predicting f_{cc} and ε_{cc} (Table 6). Therefore, several RBFN models using only two parameters (i.e., f_l and f_{cp}) or three parameters (i.e., f_l, f_{cp}, and ε_{cp}) as the input variables were also developed. The architecture of those ANN models is shown in Table 2 and they also have a good performance in predicting f_{cc} and ε_{cc} (see Tables 3 and 4). For example, Fig. 4(e) demonstrates that RK14-F4(2–7-1) model using f_l and f_{cp} as the input variables had an accurate estimate of f_{cc}. Another example is RK14-E4(2–12-1) model with f_l and f_{cp} as the input variables. It could make an accurate estimate of ε_{cc} [Fig. 5(f)]. On the whole, however, the results indicate that reducing the number of inputs had a negative effect upon the prediction accuracy of f_{cc} and ε_{cc} (Table 5).

Based on the above analysis, it is feasible to simulate the f_{cc} versus f_l or ε_{cc} versus f_l relationship curves for concrete with a specific strength. For example, the RBFN simulated chart for the relationship between f_{cc} and f_l are proposed for concrete with f_{cp} of 73.4 and 47.4 MPa (Fig. 6). The experimental results are also shown in Fig. 6 for comparison. As can be seen from Fig. 6, the simulation curve demonstrates that the predicated peak stress increased with increasing confining pressure for a fixed concrete strength. Especially, the simulation curve using four input variables fitted very well to experimental data [Fig. 6(a)]. By contrast, using two input variables, the resulting simulation curve became flatter at higher confining pressure and was thus less adequate [Fig. 6(b)]. In addition, Fig. 7 shows the RBFN simulated chart for the relationship between ε_{cc} and f_l. The axial strain at peak

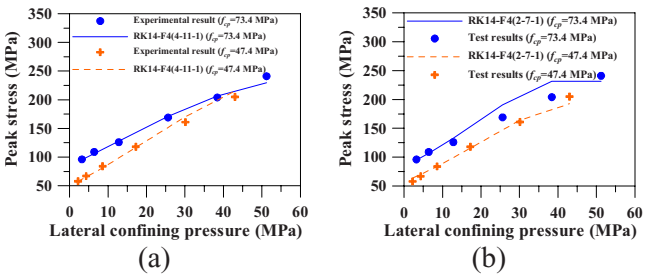

Fig. 6. RBFN simulated peak stress versus lateral confining pressure curve

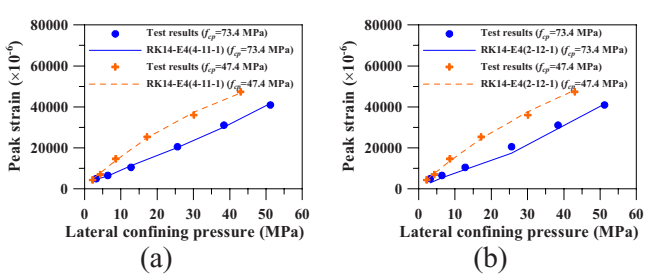

Fig. 7. RBFN simulated peak strain versus lateral confining pressure curve

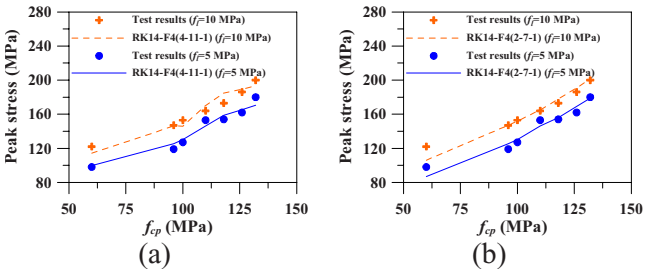

Fig. 8. RBFN simulated peak stress versus compressive strength curve

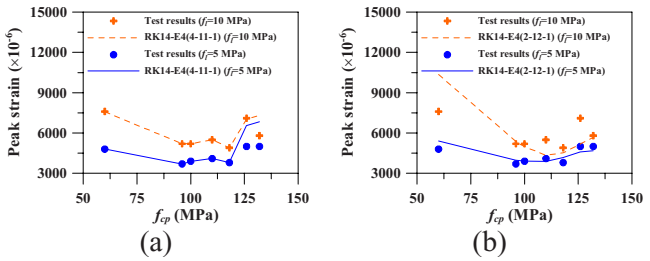

Fig. 9. RBFN simulated peak strain versus compressive strength curve

stress was shown to have a strong linear relationship with the level of confining pressure, regardless of the uniaxial strength of the concrete. Moreover, it can be observed that the simulation curves for peak strain were more satisfactory. On the other hand, the simulated f_{cc} versus f_{cp} and ε_{cc} versus f_{cp} relationship curves for a specific confining pressure are shown in Figs. 8 and 9, respectively. It is evident from Fig. 8 that the computational simulation compared well over a wide range of concrete strengths from 60 to 132 MPa. Also, it is interesting to note that the axial compressive strain at peak stress of confined concrete is a complex topic, which is a function of f_l, f_{cp}, and ε_{cp} (Fig. 9). Overall, as can be seen from Figs. 8 and 9, the use of four input variables yielded much better simulation performance since its results could be better verified with test results.

Conclusions

A comparative study has been conducted for prediction of peak stress and strain in plain concrete under triaxial stress by using neural network-based and regression-based models. However, it should be pointed out that knowledge of the stress-strain relationship of confined concrete is essential for the accurate constitutive modeling. Further studies should be performed to investigate the complete stress-strain curve of confined concrete by using ANN techniques. Based on the analytical results, the following conclusions can be drawn:

1. The use of RBFN is an appropriate and powerful tool for predicting the peak stress and strain in normal- and high-strength concretes under triaxial stress by the excellent correlation between experimental and calculated values.
2. The developed RBFN models had a good generalization performance in terms of the average RMS error and correlation coefficient values obtained from the *K*-fold cross-validation.
3. Compared with existing parametric models, the RBFN models provide better accuracy both in terms of RMS error and correlation coefficient.

Acknowledgments

The writer would like to express his appreciation for the financial support received from the National Science Council, R.O.C. under Grant No. NSC-92-2211-E-230-004.

References

Ahamd, S. H., and Shah, S. P. (1982). "Complete triaxial stress-strain curves for concrete." *Proc. Am. Soc. Civ. Eng.*, 108(4), 728–742.

Attard, M. M., and Setunge, S. (1996). "Stress-strain relationship of confined and unconfined concrete." *ACI Mater. J.*, 93(5), 433–442.

Bishop, C. M. (1997). *Neural networks for pattern recognition*, Clarendon Press, Oxford.

Candappa, D. C., Sanjayan, J. G., and Setunge, S. (2001). "Complete triaxial stress-strain curves of high-strength concrete." *J. Mater. Civ. Eng.*, 13(3), 209–215.

Cusson, D., and Paultre, P. (1995). "Stress-strain model for confined high-strength concrete." *J. Struct. Eng.*, 121(3), 468–477.

El-Dash, K. M., and Ahmad, S. H. (1995). "A model for stress-strain relationship of spirally confined normal and high-strength concrete columns." *Mag. Concrete Res.*, 47(171), 177–184.

Ghaboussi, J., Garrett, J. H., and Wu, X. (1991). "Knowledge-based modeling of material behavior with neural networks." *J. Eng. Mech.* 117(1), 129–134.

Haykin, S. (1999). *Neural networks: A comprehensive foundation*, Prentice-Hall, Upper Saddle River, N.J.

Imran, I., and Pantazopoulou, J. (1996). "Experimental study of plain concrete under triaxial stress." *ACI Mater. J.*, 93(6), 589–601.

Jain, A., Jha, S. K., and Misra, S. (2008). "Modeling and analysis of concrete slump using artificial neural networks." *J. Mater. Civ. Eng.*, 20(9), 628–633.

Jang, J. S. R., Sun, C. T., and Mizutani, E. (1997). *Neuro-fuzzy and soft computing*, Prentice-Hall, Englewood Cliffs, N.J.

Lokuge, W. P., Sanjayan, J. G., and Setunge, S. (2005). "Stress strain model for laterally confined concrete." *J. Mater. Civ. Eng.*, 17(6), 607–616.

Mander, J. B., Priestly, M. J. N., and Park, R. (1988). "Observed stress-strain behavior of confined concrete." *J. Struct. Eng.*, 114(8), 1827–1849.

Mei, H., Kiousis, P. D., Ehsani, M. R., and Saadatmanesh, H. (2001). "Confinement effects on high-strength concrete." *ACI Struct. J.*, 98(4), 548–553.

Menétrey, Ph., and Willam, K. (1996). "Triaxial failure criterion for concrete and its generalization." *ACI Struct. J.*, 92(3), 311–318.

Mindness, S., Young, J. F., and Darwin, D. (2003). *Concrete*, Prentice-Hall, Englewood Cliffs, N.J.

Moody, J. E., and Darken, C. J. (1989). "Fast learning in networks of locally-tuned processing units." *Neural Comput.*, 1(2), 281–294.

Nielsen, C. V. (1998). "Triaxial behavior of high-strength concrete and mortar." *ACI Mater. J.*, 95(2), 144–151.

Razvi, S., and Saatcioglu, M. (1999). "Confinement model for high-strength concrete." *J. Struct. Eng.*, 125(3), 281–289.

Richart, F. E., Brandtzage, A., and Brown, R. L. (1928). "A study of the failure of concrete under combined compressive stresses." *Bull. No. 185*, Engineering Experimental Station, Univ. of Illinois, Urbana, Ill.

Rumelhart, D. E., Hinton, G. E., and Williams, R. J. (1986). "Learning internal representation by error propagation." *Nature (London)*, 323, 533–536.

Sfer, D., Carol, I., Gettu, R., and Etse, G. (2002). "Study of the behavior

of concrete under triaxial compression." *J. Eng. Mech.*, 128(2), 156–163.

Sheikh, S. A., and Toklucu, M. T. (1993). "Reinforced concrete columns confined by circular spirals and hoops." *ACI J.*, 90(5), 542–553.

Tang, C. W., Chen, H. J., and Yen, T. (2003). "Modeling the confinement efficiency of reinforced concrete columns with rectilinear transverse steel using artificial neural networks." *J. Struct. Eng.*, 129(6), 775–783.

Tang, C. W., Lin, Y., and Kuo, S. F. (2007). "Investigation on correlation between pulse velocity and compressive strength of concrete using ANNs." *Comput. Concr.*, 4(6), 437–456.

Vapnik, V. (1998). *Statistical learning theory*, Wiley, New York.

Wang, C. Z., Guo, Z. H., and Zhang, X. Q. (1987). "Experimental investigation of biaxial and triaxial compressive concrete strength." *ACI Mater. J.*, 84, 92–100.

Yeh, I. C. (1999). "Design of high-performance concrete mixture using neural networks and nonlinear programming." *J. Comput. Civ. Eng.*, 13(1), 36–42.

Zhao, Z., and Ren, L. (2002). "Failure criterion of concrete under triaxial stresses using neural networks." *Comput. Aided Civ. Infrastruct. Eng.*, 17(1), 68–73.